PCCP

Accepted Manuscript

This is an *Accepted Manuscript*, which has been through the Royal Society of Chemistry peer review process and has been accepted for publication.

Accepted Manuscripts are published online shortly after acceptance, before technical editing, formatting and proof reading. Using this free service, authors can make their results available to the community, in citable form, before we publish the edited article. We will replace this *Accepted Manuscript* with the edited and formatted *Advance Article* as soon as it is available.

You can find more information about *Accepted Manuscripts* in the Information for Authors.

Please note that technical editing may introduce minor changes to the text and/or graphics, which may alter content. The journal's standard Terms & Conditions and the Ethical guidelines still apply. In no event shall the Royal Society of Chemistry be held responsible for any errors or omissions in this *Accepted Manuscript* or any consequences arising from the use of any information it contains.

www.rsc.org/pccp

PCCP

Dynamic Article Links ▶

ARTICLE TYPE

Near-Threshold Photodissociation Dynamics of CHCl₃

Mike Reid,[a,b,c] **Victoria Green,**[a,b] **and Sven P. K. Koehler***[a,b,c]

5 Energy- and angle-resolved photofragment distributions for ground-state Cl ($^2P_{3/2}$) and spin-orbit excited Cl* ($^2P_{1/2}$) have been recorded using the velocity map imaging technique after photodissociation of chloroform at wavelengths of 193 and ~235 nm. Translational energy distributions are rather broad and peak between 0.6 and 1.0 eV. The spin-orbit branching ratios [Cl*]/[Cl] are 1 and 0.3 at 193 and 235 nm, respectively, indicating the involvement of two or more excited state surfaces. Considering the anisotropy
10 parameters and branching ratios collectively, we conclude that the reaction at 193 nm takes place predominantly on the $^1Q_1$ surface, while the $^3Q_1$ surface gains importance at lower dissociation energies around 235 nm.

1. Introduction

Chloroform is best known as an anaesthetic frequently utilised in
15 the 19th century, but its usage as an anaesthetic has been discontinued around 100 years ago.[1] In synthetic chemistry, chloroform is a popular solvent,[2] and its deuterated analogue CDCl₃ is the most common solvent in NMR spectroscopy.[3] CHCl₃ is also used as a precursor in the production of
20 polytetrafluoroethylene (PTFE), and is related to some of the (hydro)chlorofluorocarbons such as CFC-11 and HCFC-22.[4]
Traces of chloroform can be found in the atmosphere and troposphere[5] from anthropogenic, but also from natural sources.[4,6] While tropospheric chloroform reacts with OH
25 radicals,[7,8] photolysis of stratospheric chloroform can produce Cl radicals (Ref. 6) which significantly contribute towards ozone depletion through the well-known chlorine cycle.[9]
The absorption spectrum of chloroform shows a broad peak centred around 175 nm which corresponds to a σ* ← n
30 transition,[10] generally referred to as the *A* band. This transition involves the excitation of a non-bonding electron on a chlorine atom to an antibonding orbital on the C–Cl bond, leading to homolytic dissociation along this bond.[11] While the stepwise reaction to form HCl is energetically more favourable, Cl radical
35 production is the only primary process under single-collision conditions.[12] The observed production of H atoms is due to subsequent photodissociation of the corresponding CHCl₂ radical, which can also serve as a hydrogen source to form HCl under high-pressure conditions.[13] With a C–Cl bond strength of
40 ~3.25 eV,[14] a 200 nm photon is sufficient to dissociate CHCl₃, which happens with a quantum efficiency Φ=1.[12]
In this paper, we report the photodissociation dynamics of CHCl₃ in a molecular beam using the velocity map imaging technique (VMI)[15] with the aim to extract angularly resolved kinetic energy
45 distributions of chlorine atoms in both spin-orbit states, Cl($^2P_{3/2}$) and Cl*($^2P_{1/2}$), and to determine the [Cl*]/[Cl] branching ratio.

Chlorine atoms are detected using a (2 + 1) REMPI (resonance-enhanced multi-photon ionisation) scheme at around 235 nm, and this wavelength is also used as a dissociation laser in the one-
50 colour experiments, while a 193 nm excimer laser is used for the two-colour experiments. Making sure to work in the linear regime (i.e. one-photon absorption only), this gives an available excess energy of 3.2 eV for 193 nm (2.0 eV for 235 nm photolysis) for Cl production, and 0.11 eV less for Cl* production, respectively.
55 At this point, it is worth describing the potential energy surfaces involved in the UV photodissociation of alkyl halides qualitatively. The ground-state of pseudo-diatomics such as monohalomethane (CH₃–X) is according to Mulliken an N state with A₁ symmetry (or a X $^1\Sigma^+$ state in diatomic notation).[16] The
60 excited states are $^1Q_1$, $^3Q_1$, $^3Q_{0^+}$, $^3Q_{0^-}$, and $^1Q_2$, however, transitions to the latter two are not dipole allowed. This leaves the $^1Q_1$ and $^3Q_1$ states with E and the $^3Q_0$ with A₁ symmetry, respectively; this leads to perpendicular ($^1Q_1$ and $^3Q_1$) and parallel ($^3Q_0$) transitions from the ground state.[17] The $^1Q_1$ and $^3Q_1$
65 states correlate adiabatically to X atoms at infinite separation, while the $^3Q_0$ excited state correlates to X* atoms, which are 882 cm^{-1} higher in energy in case of chlorine.[18]
Monohalomethanes have C_{3v} symmetry, and the main symmetry axis of the molecule overlaps with the CH₃–X bond to be broken.
70 The symmetry does initially not change during the dissociation if the halogen moves along the main symmetry axis. While trihalomethanes such as chloroform, CHCl₃, which also have C_{3v} symmetry, are at first glance similar, the main symmetry axis is not parallel to the C–X bond to be broken. This means that as
75 soon as the C–X bond stretches, the symmetry of the molecule is reduced. In chloroform, the angle between the C–Cl bond and the main symmetry axis is 72°,[19] approximated here to $\chi = \pi - \alpha_{tetr} = 70.53°$ where α_{tetr} is the angle in a non-distorted tetrahedron. If χ is the angle between the transition dipole
80 moment (along C_{3v}) and the recoil vector (along the C–Cl bond in case the axial recoil approximation is valid), then the anisotropy parameter β can be written as $\beta = 2P_2(\cos\chi)$ where P_2 is the

second order Legendre polynomial.[20] Using the approximate angle above results in an anisotropy parameter β of $-2/3$ for a transition polarised along the main symmetry axis ($A_1 \leftarrow A_1$), and $1/3$ for the transition perpendicular to it ($E \leftarrow A_1$);[21] this narrow range makes the interpretation of anisotropy parameters more ambiguous than for the monohalomethanes for which the anisotropy parameter can take the theoretical values of $+2$ for a parallel and -1 for a perpendicular transition.

The dissociation dynamics of monohalomethanes such as CH_3I, CH_3Br, and CH_3Cl have been studied more extensively than those of the trihalomethanes, probably due to their higher symmetry (producing a 'pseudo-atom' such as CH_3 rather than CHX_2 fragments); the absorption maxima in the A-band shift to lower energies in the order CH_3Cl, CH_3Br, and CH_3I, as expected. The latter has been studied most extensively both experimentally and theoretically; anisotropy parameters for the spin-orbit excited I* are close to $+2$, indicating excitation mainly to the $^3Q_0$ state. This conclusion is also enforced by the measured I*/I ratios which in all studies are >2.5 as the $^3Q_0$ state adiabatically correlates with the I* channel.[22] An anisotropy parameter only slightly reduced in value ($\sim$1.7) for the I channel indicates that curve-crossing from the $^3Q_0$ state (initial parallel transition) to the $^1Q_1$ state takes place. Curve-crossing is made possible by a deviation from C_{3v} geometry (to C_S) when the C–I bond no longer overlaps with the main symmetry axis. This bending motion of the C–I bond away from the symmetry axis also leads to rotational excitation of the resulting CH_3 radical, which has been found to be rotationally hotter in the I channel, i.e. after curve crossing, than in the I* channel.[23] Curve-crossing from $^3Q_0$ to $^1Q_1$ and the associated sudden change in geometry also favour excitation of the CH_3 umbrella mode in the I($^2P_{3/2}$) channel.[24,25] Selection rules that normally forbid singlet-to-triplet excitation (i.e. to the ^3Q states) are weakened in the case of CH_3I due to the heavy atom effect.[17] The above conclusions based on photodissociation experiments had actually been predated by the work of Gedanken and Rowe who studied the monohalomethanes CH_3I, CH_3Br, and CH_3Cl by magnetic circular dichroism (MCD) spectroscopy and demonstrated that the main absorption band in CH_3I is due to excitation to the $^3Q_0$ state.

This situation changes when moving to the lighter CH_3Br; anisotropy parameters show more perpendicular character, and while excitation to the $^3Q_0$ state still takes place, the $^1Q_1$ gains importance.[26] Br*/Br branching ratios also indicate the involvement of the $^1Q_1$ the state which correlates directly to ground state Br atoms. At the very red edge of the absorption spectrum, however, Kitsopoulos and co-workers extracted partial absorption cross sections and concluded that the $^3Q_0$ and the $^3Q_1$ states dominate.[27]

It hence comes as a surprise that the photodissociation of the yet lighter CH_3Cl molecule has been assumed to proceed via the $^3Q_0$ state for some time,[28,29] even though early MCD experiments by Gedanken and Rowe indicated that excitation to the $^1Q_1$ surface is the dominant pathway. However, later imaging studies are in line with the MCD experiments by measuring a predominantly perpendicular transition (-0.46 for Cl and -0.74 for Cl*), i.e. to the $^1Q_1$ surface, at 193 nm.[30]

Literature on the photodissociation of trihalomethanes is much sparser than that for the mono-substituted derivatives; this is probably due to the simpler CH_3 fragment in monohalomethanes, making the photodissociation a quasi-diatomic process, and the level of detail known about monohalides has neither experimentally nor theoretically been achieved for the dissociation dynamics of trihalomethanes.

The dissociation of iodoform at around 300 nm shows an anisotropy parameter of 0.46, indicating a perpendicular transition to the $^1Q_1$ state.[31] As for bromoform, McGivern et al. interpreted their isotropic angular distribution of Br atoms after 193 nm photolysis as a sign of a perpendicular transition,[32] while Jackson and co-workers obtained angular distribution that can be described by $\beta = 0.5$ (for Br, due to an avoided crossing) and 1 for Br*, albeit at a longer wavelength of 267 nm.[33]

The dissociation dynamics of $CHCl_3$ have previously been investigated using a variety of techniques, but delivered partly conflicting results. Moreover, none of the previous studies reported the combined measurement of energy distributions, anisotropy parameters, and branching ratios.

There is some agreement with regards to the Cl*/Cl spin-orbit branching ratios at 193 nm which has been determined to be 0.25 by Matsumi et al.,[34] 0.43 for ^{35}Cl as measured by Deshmukh and Hess,[35] and 0.32 by Taketani et al. using VUV-Laser Induced Fluorescence.[12] This value is significant as it shows that both states Cl and Cl* are populated, and hence that at least two excited state surfaces are involved in the dissociation dynamics.

While not being able to distinguish between Cl($^2P_{3/2}$) and Cl*($^2P_{1/2}$) atoms using photofragment translational spectroscopy, Huber and co-workers concluded that the two excited state surfaces involved are the $^3Q_0$ and the $^1Q_1$ states.[36] This is due to the fact that in the limit of a fast dissociation, the negative anisotropy parameter of the parallel transition to $^3Q_0$ and the positive anisotropy parameter of the perpendicular transition to $^1Q_1$ result in the almost isotropic distribution of 0.0 ± 0.1 of chlorine fragments measured by Huber and co-workers at 193 nm. It is expected that the $^3Q_0$ surface is less dominant in chloromethanes where a singlet-singlet transition (i.e. to the $^1Q_1$ state) is expected to gain importance due to the more strongly enforced spin-conservation rules.[37] The only other measurement of the anisotropy parameter β was performed by Kawasaki and co-workers, albeit for CDCl3 at the slightly longer wavelength range between 205 and 209 nm.[38] Their measurements indicate a perpendicular transition with anisotropy parameters (reported for Cl($^2P_{3/2}$) only) increasing from around 0.3 at low kinetic energies up to 0.7 at high kinetic energies.

The kinetic energy distributions of the chlorine fragments vary quite significantly between the various experimental investigations at 193 nm. Huber's work delivered high-resolution kinetic energy distributions of the chlorine fragments and found that 43% of the available energy is channelled into translation, with a unimodal distribution of Cl atoms peaking at around 0.94 eV (or 29% of the available energy).[36] Matsumi et al. used Doppler-resolved REMPI spectroscopy to establish an average Cl($^2P_{3/2}$) kinetic energy release of only 0.54 eV (17% of $E_{avail.}$).[21]

In the slightly longer wavelength range from 205-209 nm, Kawasaki and co-workers measured chlorine kinetic energy distribution after CDCl3 dissociation using the VMI technique
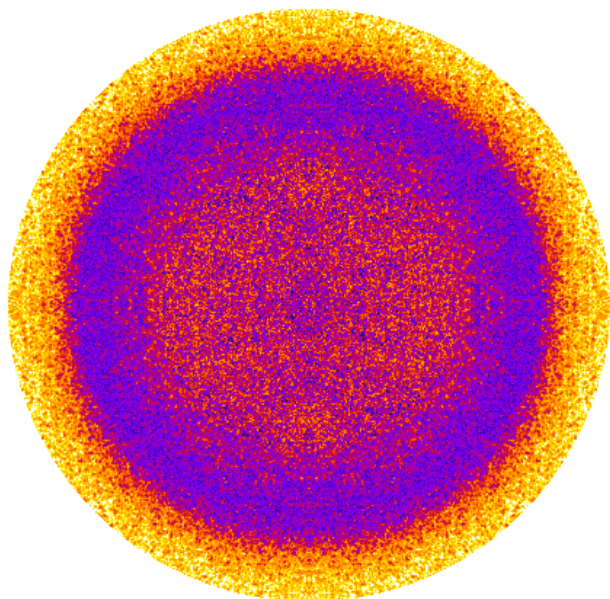
Fig. 1 Velocity-mapped image of spin-orbit ground state Cl atoms after 193 nm photolysis of chloroform, CHCl₃. The polarisation of the photolysis laser is vertical. Blue is most intense, yellow least intense.

Fig. 2 Translational energy distributions of Cl and Cl* fragments after 193 and 235 nm photodissociation of chloroform, CHCl₃. All distribution are scaled to an integral of 1.

which are rather broad and extend past 2.7 eV, showing that some two-photon processes take place.[38] They fitted their distribution to the sum of a Gaussian (centred at 1.39 eV) and a Maxwell-Boltzmann distribution (with a temperature of 7000 K) in a ratio of 40:60. Most importantly, their kinetic energy distribution stretches from >4 eV all the way to 0 eV (and shows some population at low energies), while the distributions by Huber and co-workers[36] and Matsumi *et al.*[21] gradually decline towards low kinetic energies.

Wolfrum and co-workers investigated the photodissociation dynamics of various chloromethanes at 193 nm,[13,39] but their study of chloroform dissociation focussed on the production of H atoms.[13] Their main finding directly relevant to the current study is that H atom production from CHCl₃ is not a primary channel, but instead a result of the secondary photodissocation of CHCl₂ produced in the first step. Equally, the formation of CH radicals from the 193 nm photodissociation of chloroform as studied by Romanzin *et al.* using cavity ring-down spectroscopy is not a primary single-photon process but either involves the absorption of two photons, or a sequential mechanism *via* the CHCl₂ radical.[40]

Kulshreshtha and co-workers studied the photodissociation of chloroform but at the longer wavelength of 355 nm.[41] This photon energy is slightly below the dissociation energy of the C–Cl bond in chloroform, and hence multi-photon processes are responsible for sequential Cl abstraction at this wavelength.

In light of the widely varying translational energy distributions of chlorine fragments and the fact that no previous study has reported translational and angular distributions combined with [Cl*]/[Cl] branching ratios, we here report such investigations into the photodissociation dynamics of jet-cooled chloroform at the wavelengths 193 and 235 nm. As shown below, the results obtained lead us to include in our conclusions the previously often unconsidered $^3Q_1$ potential energy surface to rationalise the
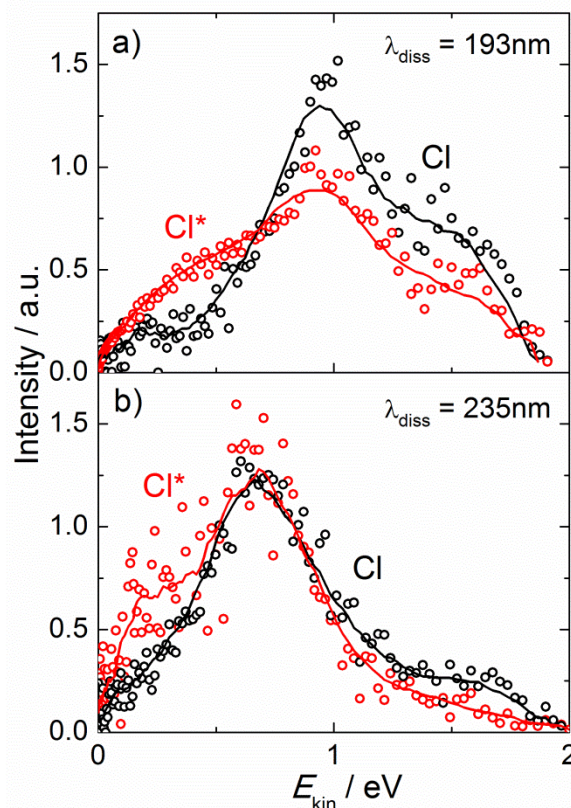
dissociation dynamics at the red edge of the absorption spectrum.

2. Experimental

Our VMI spectrometer has been described in detail before, hence only a summary will be given here.[42] A molecular beam is crossed at right angle with two counter-propagating laser beams, namely the photolysis and the probe laser, before ions are extracted along a time-of-flight tube (in line with the molecular beam axis) towards a position-sensitive detector. The molecular beam is formed by supersonic expansion of a ~5 % mixture of chloroform, CHCl₃ (Sigma-Aldrich, anhydrous, ≥99 %), in He through a General Valve nozzle at a stagnation pressure of 2.5 bar. The vapour pressure of chloroform is sufficient to mix CHCl₃ vapour with He gas prior to running experiments. The mixture passes some copper wool within the gas-line prior to reaching the nozzle to remove trace amounts of Cl₂ in the mixture. A skimmer mounted 18 mm away from the nozzle exit separates the molecular beam from the target chamber, both evacuated by 1000 l/s turbomolecular pumps. The molecular beam enters the ion optics through a 2 mm diameter central hole in the first plate, which has an overall diameter of 10 cm. The CHCl₃ molecules are dissociated using an Excimer laser (Questek 2440) operating at 193 nm. The ~30 mJ/pulse output is incident on a single quartz window mounted at Brewster's angle such that only a small fraction (<0.8 mJ) of vertically polarized light is

reflected off the window; this reflection is brought to a focus by a 20 cm lens ~2 cm behind the molecular beam. The interaction volume of the molecular and laser beam is half-way between the first and second plate of our 12-plate VMI setup. This setup 5 guarantees weak extraction conditions in the volume where the chlorine fragments are ionised. The chlorine radicals are ionised using a REMPI scheme. The third harmonic of a Continuum Powerlite 8020 is used to pump a Radiant Dyes NarrowScan laser using Coumarin 480. The 7 ns pulses are frequency-doubled to 10 yield ~0.3 mJ of laser radiation around 235 nm, which is typically reduced to 100 μJ during two-colour experiments. The probe laser beam's polarisation is turned to vertical using a periscope and focused using a 20 cm lens. The chlorine radicals are ionised using a 2+1 REMPI scheme involving the following states:

$$Cl\ 3s^2\ 3p^4\ 4p(^2P_{3/2}) \leftarrow Cl\ 3s^2\ 3p^5(^2P_{3/2})\ \ 234.08\ nm \quad (1)$$

$$Cl\ 3s^2\ 3p^4\ 4p(^2P_{1/2}) \leftarrow Cl\ 3s^2\ 3p^5(^2P_{1/2})\ \ 237.07\ nm \quad (2)$$
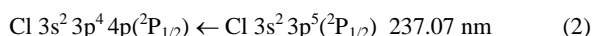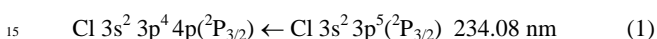
These transitions are close enough for us to be able to record the transitions consecutively without changing the laser dye, provide a strong signal in our wavelength scans, and have also previously 20 been used by other groups.[43,44] The wavelength of the tunable dye laser, that was also used as the photodissociation laser in the one-colour experiments, was scanned over the REMPI transitions during image acquisition.

The first plate (biased at 2500 V in these experiments) is one of 25 12 electrodes that make up our ion optics. A shielding cylinder surrounds all plates and part of the time-of-flight tube. The ^{35}Cl ions are detected after a 45 cm flight path by a 40 mm diameter multi-channel plate detector (Burle Photonis) coupled to a Phosphor screen. The molecular beam, photolysis and probe 30 laser, and detector are pulsed at 20 Hz as is the CCD camera which records the illuminated areas of the phosphor screen with an exposure time of 200 μs. Each image is captured on a PC and accumulated to yield the overall image ready for analysis. Calibration of the images was done by comparison with Cl_2 35 photolysis at 351 nm under otherwise identical conditions, which yielded a peak kinetic energy of 0.51 eV and a β parameter of −0.87 in close agreement with previous studies.[45]

3. Results and Discussion

40 Velocity-mapped images of Cl and Cl* atoms after photodissociation of $CHCl_3$ at 193 and ~235 nm were recorded, and an image of ground-state Cl fragments after 193 nm dissociation is shown in Fig. 1. These images were converted to speed distributions using BASEX and subsequently to kinetic 45 energy distributions, see Fig. 2, after application of the appropriate Jacobian transformation.[46,47] Kinetic energy distributions after 193 nm dissociation predominantly peak at around 1 eV (31% of the overall available energy); this value is in excellent agreement with the distributions measured by Huber 50 and co-workers.[36] The average kinetic energy for the Cl* channel is ~0.08 eV lower than that for Cl, which fits the spin-orbit splitting of 0.11 eV well at a counterfragment mass of 84 amu ($CHCl_2$) and a parent mass of 119.5 amu. Our distributions are broader than those measured by Huber, similar to those measured 55 by Matsumi *et al.*, but narrower than those measured by Mashino
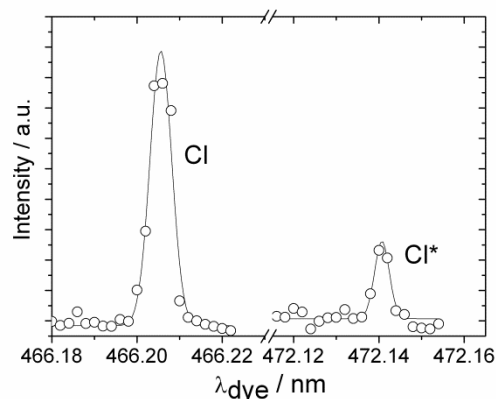
Fig. 3 Measurement of branching ratio [Cl*]/[Cl] after 235 nm photolysis of chloroform, $CHCl_3$. Each line is the average of five scans and fitted to a Gaussian before integration. Areas underneath each line scaled to 60 represent the measured branching ratio of 0.3.

et al., albeit the latter were measured after photodissociation at ~205 nm. For both 193 and 235 nm dissociation, intensities in the distributions decrease notably when going to low kinetic energies, indicating (together with the structureless $CHCl_3$ 65 absorption spectrum, see Ref. 11) an excitation to a repulsive excited state. These characteristics of a direct dissociation on a repulsive state also enforce our assumption of the sudden recoil approximation, i.e. the parent molecule dissociating rapidly on the timescale of molecular rotation. However, we speculate that 70 the wider kinetic energy distributions as compared to Huber could be due to the $CHCl_2$ radical absorbing a second photon to produce another chlorine atom with unknown energy distribution,[40,48] or due to a small amount of clustering within our cooled beam due to the relatively high chloroform concentration 75 necessary due to the low absorption cross section.[49]

We measured the ion signal as a function of the 193 nm pulse energy and arrive at a linear relationship (slope of the log-log plot 0.95±0.11), while the slope for the 235 nm dissociation experiments is 2.85±0.18. We believe that the measured energy 80 distributions even at ~235 nm are predominantly a result of one-photon excitations. The lower Cl kinetic energies (~0.7 eV or 35% of the available energy) after 235 nm dissociation do not fully account for the difference in photon energy, but a two-photon process at 235 nm would add noticeably more energy to 85 the system than at 193 nm, and we do not see evidence for this in our images. Instead, we conclude that the $CHCl_2$ counter-fragment carries less internal energy after 235 nm than after 193 nm dissociation. At a total energy release of ~2 eV after 235 nm photolysis, we calculate the $CHCl_2$ fragment internal 90 energy to be ~1 eV, while it is around 1.7 eV after 193 nm photolysis. The latter value corresponds to 46% of excess energy being channelled into translation which is in excellent agreement with the work by Huber and co-workers who determined this value to be 43% using photofragment translational 95 spectroscopy.[36] The two-photon fragment energies as measured by Kawasaki and co-workers extend to much higher energies,[38] further enforcing our conclusion that the results presented here are due to single-photon excitation.

Angular distributions were fitted to a function of the form

$$I(\theta) = [1 + \beta\, P_2\,(\cos\theta)] / 4\pi \qquad (3)$$

where P_2 is the second-order Legendre polynomial. Anisotropy parameters β were determined for Cl and Cl* after 193 and 235 nm photolysis for all fragment energies, but the values were rather scattered for those energies with little population. However, the average β values over all energies were greater than zero for the three combinations Cl*/193 nm, Cl/235 nm, Cl*/235 nm, and around zero for Cl/193 nm. The values shown in Table 1 are averaged only over those chlorine fragments covered by the full-width half-maximum around the peak energies of the energy distributions due to the better S/N. If the dissociation process is much faster than the timescales of molecular rotation, i.e. any influence of molecular rotation can be excluded, then deviations from the predicted anisotropy parameters are a sign of the involvement of multiple potential energy surfaces.[21]

The [Cl*]/[Cl] branching ratios were determined by integrating the area when scanning over the REMPI transitions used for Cl* and Cl detection, and calculating their ratio, see Fig. 3. However, in order to exclude detection efficiency errors (arising from different line strengths, varying degrees of saturation,…), we also measured these ratios for 351 nm photodissociation of Cl_2 for which branching ratios have been determined previously.[50] We thus apply a scaling factor to the calculated ratios of areas to arrive at the corrected branching ratios, see Table 1.

$$\frac{[Cl^*]}{[Cl]} = \frac{I_{Cl*}(CHCl_3)}{I_{Cl}(CHCl_3)} \times \frac{\frac{[Cl*]}{[Cl]}(Cl_2)}{\frac{I_{Cl*}}{I_{Cl}}(Cl_2)} \qquad (4)$$

Table 1: Anisotropy parameters β for Cl and Cl* and branching ratios [Cl*]/[Cl] as a function of photolysis wavelength

		193 nm	235 nm
Anisotropy parameter β	Cl	-0.05±0.1	0.2±0.1
	Cl*	0.3±0.1	0.3±0.2
Branching ratio	[Cl*]/[Cl]	1.0±0.1	0.3±0.1

Kawasaki and co-workers measured an anisotropy parameter of around 0.3 for Cl at the slightly longer wavelength of 205 nm, but no value for Cl* was reported,[38] while Bersohn and co-workers measured an almost isotropic angular distribution for both spin-orbit states.[21] However, the geometry of chloroform with the C–Cl bond not being parallel to the main axis of symmetry already limits the anisotropy parameters to values in the narrow range between 1/3 and –2/3. This smaller range makes the interpretation of anisotropy parameters less distinct, even more so as the values measured in this work span an even narrower range roughly between ~0 and +0.3.

However, combined with the branching ratios, we can draw the following picture for 235 nm dissociation: β parameters close to the limiting value for both spin-orbit states indicate excitation predominantly to either the $^1Q_1$ or the $^3Q_1$ state. We include the lowest-lying state, $^3Q_1$, in our analysis, which is reasonable in the red part of the absorption spectrum, and is in agreement with conclusions in previous work on bromohalomethanes.[27] Both states correlate with ground-state Cl atoms in accordance with a

Cl population of around 80%, and since they have the same theoretical anisotropy parameter, one cannot further quantify the contribution from each state. The small population of Cl* can be explained either by including some excitation to the $^3Q_0$ state which would rationalise the slightly lower anisotropy parameter of 0.2, or by some curve-crossing from $^1Q_1$ and $^3Q_0$.

At 193 nm, those 50% of chloroform molecules that produce Cl* atoms ([Cl*]/[Cl] = 1) are primarily (96%) excited to the $^1Q_1$ surface ($\beta = 0.3$) but undergo curve-crossing to the $^3Q_0$ surface, resulting in spin-orbit excited Cl* atoms.[51] Excitation to the $^3Q_1$ surface would also account for an anisotropy parameter of ~0.3, but that state does not cross the $^3Q_0$ surface to produce Cl* atoms. When adopting the theoretical β parameters derived by Bersohn for chloroform,[21] the almost isotropic Cl distribution at 193 nm ($\beta = -0.05$) indicates that 62% of the Cl ($^2P_{3/2}$) atoms are due to perpendicular transitions, and 38% due to parallel transitions, according to

$$\beta(Cl) = a_\perp \beta_\perp + (1 - a_\perp)\beta_\parallel. \qquad (5)$$

If one further assumes that the contribution of the $^3Q_1$ state is negligible at this lower wavelength of 193 nm, one can identify four different pathways as shown in Table 2.

Table 2 Relative probabilities for the four pathways following 193 nm excitation of chloroform

	transition	final spin-orbit state	probability
$f(^3Q_0)$	$\parallel$	Cl*	0.02
$f(^3Q_0 \to {}^1Q_1)$	$\parallel$	Cl	0.19
$f(^1Q_1 \to {}^3Q_0)$	$\perp$	Cl*	0.48
$f(^1Q_1)$	$\perp$	Cl	0.31

Following the procedure of Jung and co-workers and Townsend et al.,[52,30] and recognising that the [Cl*]/[Cl] branching ratio of unity equates to a quantum yield of 0.5 for each spin-orbit state, one can quantify that 31% of the chloroform molecules are excited to the $^1Q_1$ state to form ground-state chlorine atoms ($f(^1Q_1)$), and 19% are excited to the $^3Q_0$ state but emerge as Cl atoms after curve crossing ($f(^3Q_0 \to {}^1Q_1)$). In quantifying the two channels leading to the 50% of Cl* atoms with $\beta = 0.3$ discussed qualitatively above, pathway $f(^1Q_1 \to {}^3Q_0)$ contributes 48% overall while direct excitation to $^3Q_0$ without curve-crossing only contributes 2%. This yields curve-crossing probabilities after excitation to the $^3Q_0$ state of 8% ($f(^3Q_0 \to {}^1Q_1)$ / [$f(^3Q_0 \to {}^1Q_1)$ + $f(^3Q_0)$]), and of 61% for the $^1Q_1 \to {}^3Q_0$ pathway ($f(^1Q_1 \to {}^3Q_0)$ / [$f(^1Q_1 \to {}^3Q_0)$ + $f(^1Q_1)$]). It is necessary to point out that while our branching ratio at 235 nm is close to previous measurements, the branching ratio at 193 nm is higher. However, our conclusion that excitation at 193 nm proceeds primarily ($f(^1Q_1 \to {}^3Q_0)$ + $f(^1Q_1)$ = 79%) to the $^1Q_1$ state is mainly based on the anisotropy parameters, and is in line with the prediction that the lighter chlorine compounds are less likely to induce a breakdown of the spin selection rules, and that hence singlet-singlet transitions should be preferred.[17]

We note that a small component (17%) of the 193 nm Cl* kinetic energy distributions at around 1.5 eV (see Fig. 2) has a β parameter close to zero rather than ~0.3 for the main peak; we speculate that there is some excitation directly to the $^3Q_0$ state at

these higher fragment energies, and that these faster fragments are less likely to undergo curve-crossing.

Conclusions

We have measured the photodissociation dynamics of chloroform at 193 and ~235 nm using the VMI technique. Chlorine fragment kinetic energy distributions, anisotropy parameters, and spin-orbit branching ratios were determined. We established that excitation to repulsive states is the first step in the dissociation process, however, we also see a minor component due to secondary dissociation at higher kinetic energies, and a component likely due to clustering at kinetic energies lower than the main contribution. As for the primary channel after dissociation at 235 nm, around half of the available excess energy goes into translation, with the other half going into internal degrees of freedom, and this ratio is slightly lower for 193 nm dissociation.

The dissociation dynamics of chloroform have so far been identified as being dominated by the $^1Q_1$ state,[38] or as involving the two excited states $^1Q_1$ and $^3Q_0$.[36] The $^3Q_0$ state is the only state to correlate with spin-orbit excited chlorine atoms, but it is identifiable as it is also the only state involving a parallel transition. Our anisotropy parameters, in particular those for 235 nm dissociation, indicate that the $^3Q_0$ state does not seem to play as big a role as observed in other alkyl chlorides, especially at longer wavelengths; instead excitation to the $^3Q_1$ state gains importance. Population in spin-orbit excited Cl* is instead mainly due to curve-crossing from $^1Q_1$ to $^3Q_0$. Dissociation at 193 nm involves excitation to both the $^1Q_1$ (79%) and $^3Q_0$ (21%) states as can be seen from the higher branching ratio and the almost isotropic angular distribution of the Cl products.

When going to longer wavelengths, the fact that the [Cl*]/[Cl] branching ratio decreases and the anisotropy parameters increase on average further enforces our conclusion that the first excited $^3Q_1$ state plays a role in the dissociation at the red edge of the absorption spectrum.[25,53]

Notes and references

a School of Chemistry, The University of Manchester, Manchester M13 9PL, UK. Tel: +44 161 306 4448
b Photon Science Institute, The University of Manchester, Manchester M13 9PL, UK.
c Dalton Cumbrian Facility, The University of Manchester, Moor Row, Whitehaven CA24 3HA, UK
* *E-mail: sven.koehler@manchester.ac.uk*

† Electronic Supplementary Information (ESI) available: [details of any supplementary information available should be included here]. See DOI: 10.1039/b000000x/

1 W. E. Burge, *Science*, 1917, **46**, 618; Anonymous, *Science*, 1885, **6**, 154.
2 G. M. Barrow and E. A. Yerger, *J. Am. Chem. Soc.*, 1954, **76**, 5211.
3 V. Madison and K. D. Kopple, *J. Am. Chem. Soc.*, 1980, 102, 4855.
4 M. L. Aucott, A. McCulloch, T. E. Graedel, G. Kleinman, P. Midgley and Y.-F. Li, *J. Geophys. Res.*, 1999, **104**, 8405.
5 F. S. Rowland and M. J. Molina, *Rev. Geophys.*, 1975, **13**, 1.
6 M. A. K. Khalil, R. M. Moore, D. B. Harper, J. M. Lobert, D. J. Erickson, V. Koropalov, W. T. Sturges and W. C. Keene, *J. Geophys. Res.*, 1999, **104**, 8333.
7 H. B. Singh, L. J. Salas, H. Shigeishi and W. Scribner, *Science*, 1979, **203**, 899.
8 S. O'Doherty, P. G. Simmonds, D. M. Cunnold, H. J. Wang, G. A. Sturrock, P. J. Fraser, D. Ryall, R. G. Derwent, R. F. Weiss, P. Salameh, B. R. Miller and R. G. Prinn, *J. Geophys. Res.*, 2001, **106**, 20429.
9 M. J. Molina and F. S. Rowland, *Nature*, 1974, **249**, 810.
10 P.C. Simon, D. Gillotay, N. Vanlaethem-Meuree, J. Wisemberg, *J. Atmos. Chem.*, 1988, **7**, 107.
11 B. R. Russell, L. O. Edwards and J. W. Raymonda, *J. Am. Chem. Soc.*, 1973, **95**, 2129.
12 F. Taketani, K. Takahashi and Y. Matsumi, *J. Phys. Chem. A*, 2005, **109**, 2855.
13 R. A. Brownsword, M. Hillenkamp, T. Laurent, R. K. Vatsa, H.-R. Volpp and J. Wolfrum, *J. Phys. Chem. A*, 1997, **101**, 5222.
14 S. P. Sander, J. Abbatt, J. R. Barker, J. B. Burkholder, R. R. Friedl, D. M. Golden, R. E. Huie, C. E. Kolb, M. J. Kurylo, G. K. Moortgat, V. L. Orkin and P. H. Wine, "Chemical Kinetics and Photochemical Data for Use in Atmospheric Studies, Evaluation No. 17," JPL Publication 10-6, Jet Propulsion Laboratory, Pasadena, 2011 http://jpldataeval.jpl.nasa.gov.
15 D. W. Chandler and P. L. Houston, *J. Chem. Phys.*, 1987, **87**, 1445; A. T. J. B. Eppink and D. H. Parker, *Rev. Sci. Instrum.*, 1997, **68**, 3477.
16 R. S. Mulliken, *Phys. Rev.*, 1937, **51**, 310; R. S. Mulliken, *J. Chem. Phys.*, 1940, **8**, 382.
17 A, Gedanken and M. D. Rowe, *Chem. Phys. Lett.*, 1975, **34**, 39.
18 A. Kramida, Y. Ralchenko, J. Reader and NIST ASD Team, 2012, NIST Atomic Spectra Database (version 5.0), http://physics.nist.gov/asd
19 M. Jen and D. R. Lide Jr., *J. Chem. Phys.*, 1962, **36**, 2525.
20 S. Yang and R. Bersohn, *J. Chem. Phys.*, 1974, **61**, 4400.
21 Y. Matsumi, K. Tonokura, M. Kawasaki, G. Inoue, S. Satyapal and R. Bersohn, *J. Chem. Phys.*, 1991, **94**, 2669.
22 W. P. Hess, S. J. Kohler, H. K. Haugen, and S. R. Leone, *J. Chem. Phys.*, 1986, **84**, 3192; F. G. Goodwin, P. A. Gorry, P. M. Hughes, D. Raybone, T. M. Watkinson, and J. C. Whitehead, *Chem. Phys. Lett.*, 1987, **135**, 163.
23 Y. Amatatsu, K. Morokuma, and S. Yabushita, *J. Chem. Phys.*, 1991, **94**, 4858.
24 R. K. Sparks, K. Shobatake, L. R. Carlson, and Y. T. Lee, *J. Chem. Phys.*, 1981, **75**, 3838.
25 Y. Amatasu, S. Yabushita, and K. Morokuma, *J. Chem. Phys.*, 1996, **104**, 9783.
26 G. N. A. van Veen, T. Baller, A. E. De Vries, N. J. A van Veen, *Chem. Phys.*, 1984, **87**, 405.
27 T. Gougousi, P. C. Samartzis, T. N. Kitsopoulos, *J. Chem. Phys.*, 1998, **108**, 5742.
28 A. Melchior, H. M. Lambert, P. J. Dagdigian, I. Bar and S. Rosenwaks, *Isr. J. Chem.*, 1997, **37**, 455.
29 H. M. Lambert, and P. J. Dagdigian, *J. Chem. Phys.*, 1998, **109**, 7810.
30 D. Townsend, S. K. Lee and A. G. Suits, *J. Phys. Chem. A*, 2004, **108**, 8106.
31 M. Kawasaki, S. J. Lee, and R. Bersohn, *J. Chem. Phys.*, 1975, **63**, 809.
32 W. S. McGivern, O. Sorkhabi, A. G. Suits, A. Derecskei-Kovacs and S. W. North, *J. Phys. Chem. A*, 2000, **104**, 10085.
33 D. Xu, J. S. Francisco, J. Huang, and W. M. Jackson, *J. Chem. Phys.*, 2002, **117**, 2578.
34 Y. Matsumi, P. K. Das, M. Kawasaki, *J. Chem. Phys.*, 1992, **97**, 5261.

35 S. Deshmukh and W. P. Hess, *J. Photochem. Photobiol. A: Chem.*, 1994, **80**, 17.

36 X. Yang, P. Felder, J. R. Huber, *Chem. Phys.*, 1994, **189**, 127.

37 A. Gedanken and M. D. Rowe, *Chem. Phys. Lett.*, 1975, **34**, 39.

38 M. Mashino. H. Yamada, A. Sugita and M. Kawasaki, *J. Photochem. Photobiol. A: Chem.*, 2005, **176**, 78.

39 A. Melchior, P. Knupfer, I. Bar, S. Rosenwaks, T. Laurent, H.-R. Volpp and J. Wolfrum, *J. Phys. Chem.* 1996, **100**, 13375.

40 C. Romanzin, B. Gans, S. Douin, S. Boyé-Péronne and D. Gauyacq, *Chem. Phys.*, 2008, **351**, 77.

41 P. Sharma, R. K. Vatsa, D. K. Maity and S. K. Kulshreshtha, *Rapid Commun. Mass Spectrom.*, 2004, **18**, 2383.

42 M. Reid and S. P. K. Koehler, *Rev. Sci. Instrum.*, 2013, **84**, 044101.

43 P. C. Samartzis, N.Hansen and A. M. Wodtke, *Phys. Chem. Chem. Phys.*, 2006, **8**, 2958.

44 H. P. Upadhyaya, A. Saha, A. Kumar, T. Bandyopadhyay, P. D. Naik, and P.N. Bajaj, *J. Phys. Chem. A*, 2010, **114**, 5271.

45 P. C. Samartzis, I. Sakellariou, T. Gougousi and T. N. Kitsopoulos, *J. Chem. Phys.*, 1997, **107**, 43.

46 V. Dribinski, A. Ossadtchi, V. A. Mandelshtam and H. Reisler, *Rev. Sci. Instrum.* 2002, **73**, 2634.

47 I. Rahinov, R. Cooper, C. Yuan, X. Yang, D. J. Auerbach and A. M. Wodtke, *J. Chem. Phys.* 2008, **129**, 214708.

48 J. H. Lehman, H. Li and M. I. Lester, *Chem. Phys. Lett.*, 2013, **590**, 16.

49 W. S. McGivern, R. Li, P. Zou, and S. W. North, *J. Chem. Phys.*, 1999, **111**, 5771.

50 Y. Matsumi, K. Tonokura and M. Kawasaki, *J. Chem. Phys.,* 1992, **97**, 1065.

51 Y.-J. Jung, M. S. Park, Y. S. Kim, K.-H. Jung, and H.-R. Volpp, *J. Chem. Phys.*, 1999, **111**, 4005.

52 T. K. Kim, M. S. Park, K. W. Lee and K.-H. Jung, *J. Chem. Phys.*, 2001, **115**, 10745.

53 D. H. Fairbrother, K. A. Briggman, E. Weitz, and P. C. Stair, *J. Phys. Chem.*, 1994, **101**, 3787.